Natural Hazards
and Earth System
Sciences
Discussions

The OBS noise due to deep ocean currents

Carlos Corela[1], Afonso Loureiro[1], José Luis Duarte[1], Luis Matias[1], Tiago Rebelo[2], Tiago Bartolomeu[2]

[1]Instituto Dom Luiz, Faculdade de Ciências, Universidade de Lisboa, 1749-016 Lisboa, Portugal
[2]CEIIA, Av. D. Afonso Henriques, 1825, 4450-017 Matosinhos, Portugal

5 *Correspondence to*: Carlos Corela (ccorela@fc.ul.pt)

Abstract. Ocean bottom seismometers (OBS) are usually deployed for seismological investigations but these objectives are impaired by noise resulting from ocean environment. We split the OBS recorded seismic noise into three domains, short-period, microseisms and long-period, also known as tilt-noise. We show that the first and third domains are controlled by bottom currents but these are not always a function of the tidal forcing. Instead we suggest that the ocean bottom has a flow
10 regime resulting from two possible contributions, the permanent low frequency bottom current and the tidal current. The recorded noise displays the balance between these two currents along the full tidal cycle, between neap and spring tides. In the short-period noise band the ocean current generates harmonic tremors that corrupt the dataset records. We show that, in the analysed cases, the harmonic tremors result from the interaction between the ocean current and mechanical elements of the OBS that are not essential for sea bottom recording and thus have no geological origin. The data from a new Broadband
15 OBS type, designed and built at Instituto Dom Luiz (University of Lisbon)/CEIIA, hiding no essential components from current flow, shows how utmost of the harmonic noise can be eliminated.

1. Introduction

Ocean Bottom seismometers (OBS) are deep-sea instruments built with the main purpose of monitoring offshore seismicity of tectonically active areas (e.g., Geissler et al., 2010; Silva et al., 2017), contribute to seismology regional and
20 global studies (e.g., Monna et al., 2013; Civiero et al., 2018; Civiero et al., 2019) and image the marine subsurface (e.g., Bowden et al., 2016; Loureiro et al., 2016; Corela et al., 2017). Typically, these instruments are dropped from a ship into the ocean, and free-fall through the water column until they reach the seafloor.

OBS measure ground motions, much like seismic stations on land do. However, deployment conditions in the seafloor are different from those in the continent as the seismmometer can be protected from environment disturbances (e.g.,
25 wind, temperature) through installations several meters underground whereas OBS stay on the seafloor exposed to all oceanic physical phenomena. This makes an OBS more than a seismic station, recording in addition to all types of seismic data (of geological, biological or anthropogenic origin), also oceanographic information (currents) as noise data. The noise of oceanic origin significantly impairs the investigation of all other phenomena leading to major challenges and technical difficulties.

30   This noise can be split into three different domains in spectrograms (Figure 1): i) The short-period band from 0.5Hz to 40Hz, which includes the "harmonic tremor" (between 0.5 and 6.5Hz) discussed and interpreted either as an instrumental cause, a geological cause or both; ii) from 2s to 20s, a well-known geophysical origin that corresponds to the microseisms domain and iii) the long-period band from 20s to 60s dominated by the tilt noise, generally attributed to currents tilting the instrument.

35   One of the challenges of seismic observations in the oceans regards the efficiency of noise reduction generated by oceanic processes (Webb, 1998). Understanding the sources and amplitudes of seismic noise in the oceans is important for improving OBS design in terms of instrumental capabilities and self-noise mitigation.

On the short-period domain, 0.5-40Hz (limited by the sampling rate of 100Hz), local seismic events, whales singing are widely recorded and long-lasting harmonic tremor signals are commonly observed in spectrograms of OBS data with
40   frequency content overlapping local earthquake signals. Such a problem has been described since the beginning of the development of OBS instruments. The first attempt to describe OBS behaviour in terms of self-noise was made near Hawaii (Duennebier et al., 1981; Lewis and Tuthill, 1981; Sutton et al., 1981a,b; Trehu and Solomon, 1981; Tuthill et al., 1981; Zelikovitz and Prothero, 1981; Trehu, 1985a,b; Duennebier et al., 1995). Some of these authors show that resonance, related to von Kármán vortex shedding off from the various parts of the instrument (a repeating pattern of swirling vortices
45   responsible for the unsteady flow separation on the several components of the OBS), can occur when near-bottom currents force the water to flow around an OBS. The current-induced noise was investigated using simultaneous recordings of ocean tides, current speed, seismic noise, and transients' tests to study cross-coupling in several instruments available at that period.

Similar results were reported by Kovachev et al., (1997), showing oscillation modes specific to the body of an OBS
50   excited by near-bottom currents. These motions affected the seismic sensor, even when the sensor compartment lies several meters away from the noise source. The presence of oscillating frequencies also affects the shape of recorded earthquakes signals as they can also cause oscillations of the mechanical components of the station. Kovachev et al. (1997) concluded that the oscillations were caused by the interaction of the OBS components with the near-bottom current flow. However, unlike the von Kármán vortex mechanism, the observed resonant frequency was independent of the current flow speed. They
55   suggested the formation of vortices on the vibrating components of the OBS as responsible for these oscillations. When the vortex shedding frequency (Strouhal frequency) was close to the resonant frequency of the station, resonant interaction between the current and mechanical station components takes place leading to an effect called wake or lock-in in literature (e.g., Skop and Griffin, 1975; Griffin, 1985; Sumer and Fredsoe, 1999, Stahler et al., 2018; Essing et al., 2021). Later on, in discussion, frequency locking or mode locking is mention to define this effect.

60   Webb (1998) also reported that noise can be locally generated by the interaction between seafloor currents and OBS components. A radio antenna or other elements such as cables attached to the OBS structure were observed to vibrate as a strummed string due to the current flow. This, in turn, produced harmonic noise with a narrow and energetic peak at frequencies of a few hertz.

2

65 Other studies reported harmonic signals in volcanic, nonvolcanic and hydrothermal regions of the world (Pontoise and Hello, 2002; Tolstoy et al., 2002; Díaz et al., 2007; Monigle et al., 2009; Bazin et al., 2010; Franek et al., 2014) associated with gas venting and/or resonance of fluid filled cracks. These studies concluded that harmonic tremors can result from sustained pressure fluctuations, probably related to stress variations induced by the tidal change of oceanic load. Research campaigns frequently report that harmonic tremor signals are often tidally modulated (Monigle et al., 2009; Franek et al., 2014; Meier and Schlindwein, 2018; Ugalde et al., 2019, Ramakrushana Reddy et al., 2020). Some of these signals

70 clearly coincide with the occurrence of earthquake swarms (Meier and Schlindwein, 2018), although almost identical to hydrodynamically induced tremor on the OBS structure (Stähler et al., 2018). Recent studies (Stähler et al., 2018, Ugalde et al., 2019, Ramakrushana Reddy et al., 2020 and Essing et al., 2021) show that modern OBS design are also susceptible to substantial hydrodynamic tremor. Stähler et al. (2018) suggest vortex shedding on protuberant objects of the OBS, such as the recovery buoy or the flagpole, as being the general excitation mechanism. Ugalde et al. (2019) observed harmonic tremor

75 in their data set and suggest resonances of the OBS-sediments coupled system as a source driven by water currents modulated by tides. Essin et al. (2021) emphasized that the tremor episodes typically occur twice per day, starting with fundamental frequencies of 0.5-1Hz showing three distinct stages that are characterized by frequency gliding, mode-locking and large spectral amplitudes. These effects are amplified when vortex-shedding frequencies match the resonance frequency of the structure or the head-buoy rope when regarded as a strummed string.

80 The second noise domain, 2-20s (Figure 1), is the microseisms noise of ocean waves origin. The primary microseism or single-frequency microseism noise (11-20s) is generated in shallow waters where the depth is less than the wavelength of wind-forced gravity waves (Bromirski et al., 2005) and has periods similar to those of the main ocean swell. The secondary microseism or double-frequency microseism noise (2–10s) is generated by the nonlinear interaction of ocean waves traveling in opposite directions (Longuet-Higgins, 1950).

85 The low frequency noise domain, 20-60s, is generally attributed to currents tilting the OBS which causes a redistribution of gravitational force between the horizontal and vertical component of the seismometer (Sutton and Duennebier, 1987; Webb, 1998; Duennebier and Sutton, 1995; Crawford and Webb, 2000; An et al., 2021). Current-induced tilt noise is generated by two processes, a displacement term due to the change in the seismometer position, and a rotation term that comes from the change in the gravitational acceleration on the seismometer. At low frequencies, the rotation term

90 dominates, which can be calculated by the gravitational acceleration and the tilt angle (Crawford and Webb, 2000). The origin and characteristics of the horizontal tilt noise remains poorly understood despite its association with ocean-bottom currents that is widely accepted (An et al., 2021). Another source for the 20-60s noise domain is the infragravity waves, which are characterize by small wave height, long wavelength and long period (30-500s), induce long-period noise (>30s) on the vertical component of the seismometer (Webb, 1998, 2007; Ardhuin et al., 2015; Doran and Laske, 2016).

95 Several hypotheses have been elaborated to explain the origin of harmonic tremors in the first noise domain. Typically, the signal from these tremors has a little or no influence on the hydrophone sensor and is only seen in the seismometer records. This study uses the vertical component of the seismometer to identify and discuss the origin of the recorded harmonic

tremors. It also presents an OBS design that mitigates the problem that we consider of instrumental origin and not generated by geological causes.

2.   Data and Methods

From September 2007 to August 2008, an ocean bottom seismometer experiment (NEAREST-NT) took place offshore of Cape S. Vincent and in the Gulf of Cádiz (Geissler et al., 2010), in the Portuguese and Moroccan exclusive economic zones, on board an Italian Ship, RV *Urania*, where 24 LOBSTER (OBS) from the German DEPAS instrument pool were deployed at depths ranging from 2000 to 5100 meters depth (Figure 2).

During this deployment, all the OBS recorded a plethora of signals (Corela PhD, 2014), however, this paper will focus the harmonic tremors and tilt noise spectral windows recorded on NT OBS01, NT OBS03 and NT OBS04 in the area between the Gorringe bank (GB) and Saint Vincente canyon (SVC) where the deep current flow influence is expected to be more pronounced due to rougher topography. NT OBS01 was located at the Tagus Abyssal plain (TAP) deployed at a depth of 5100 meters, NT OBS03 in the middle of the D. Henrique basin at a depth of 3932 meters and NT OBS04 near São Vicente Canyon at a depth of 1993 meters (Figure 2).

All instruments recorded continuously at a 100Hz sampling rate on 3-component GURALP seismometer of 60s corner period (CMG-40TOBS) and on a hydrophone HTI-04/01-PCA (Figure 3).

The LOBSTER (Alfred-Wegener-Institut, Helmholtz-Zentrum fur Polar- und Meeresforschung et al., 2017) components are illustrated in Figure 3. The seismometer, hydrophone, data recorder and batteries comprise the acquisition system while the syntactic foam floats and releaser unit are required only for recovery the instrument from the seafloor. The flag, radio beacon and flashlight are only needed when OBS surfaces and are used to locate the instrument. The head-buoy is only used to help retrieving the instrument from the sea-surface to the ship. All the elements that are not required for data recording will also be present on the seafloor connected to the instrument frame. The head-buoy floats 7-10 meters above the OBS with the 18 mm diameter rope tied to the principal OBS mainframe. The sub-horizontal flagpole has a diameter of 21mm and is 1.3 m long. The radio antenna has a diameter of 1.9 mm and is 42 cm long. Both are firmly attached to the OBS frame. The titanium mainframe has a rigid connection to the gimbaled seismometer.

In this work, we compare the performance of the NEAREST OBS with the new broadband OBS developed and built in Portugal at Instituto Dom Luiz (IDL)/CEIIA within Project DUNE (PTDC/EAM-OCE/28389/2017). The DUNE OBS (Figure 4) was deployed the 25 May 2021 and recovered the 15 October 2021 at the same position of NT OBS04 of the NEAREST campaign near the São Vicente Canyon (Figure 2) with the objective to compare the environment generated noise on the two data records despite the long-time interval between them.

The purpose of the DUNE OBS was the mitigation of the influence of the deep-sea currents on the instrument. The accessories (flag, radio antenna and head-buoy) are all inside the outer orange shell during the free-fall and recording period. After releasing the instrument from the anchor at the seafloor, the flag, radio antenna, flash beacon and head buoy are

130   released from the frame and stand outside the outer shell to simplify its recover at the surface. The seismometer (Guralp Aquarius 120s-100Hz) is firmly connected to the OBS inner structure, a similar placement as in the LOBSTER OBS.

In the deep ocean, where OBS are deployed, theoretical and numerical studies suggest that current flow is efficiently generated by deep tidal (Garrett and Kunze, 2007) and geostrophic motions (Nikurashin and Ferrari, 2010a; Nikurashin and Ferrari, 2010b) flowing over rough small-scale topography. The flow regime may have two contributions,

135   the tidal current and the permanent low frequency current. Observations showed a stark contrast between conditions at spring and neap tide. During spring tide, within the influence of new moon or the full moon, the amplitude range between low and high tide, in ebb or flood tide, reach a maximum, meaning higher tide flow speed and this term should prevail over the permanent low-frequency flow (Voet et al., 2020). Through neap tides, first and third quarter moon, the amplitude range between the low and high tide, during the ebb or flood tide, reach a minimum, meaning a low tide flow speed and the

140   permanent low-frequency flow dominates over the oscillatory tide flow (ibid.). During spring tides when oscillatory speeds are stronger the low-frequency flow will bias the resulting current flow by reducing the flow speed when interacting opposed to the tide flow and increasing when in phase (ibid.). These authors concluded that both, tides and low-frequency flows, interact with bottom topography and the energy dissipation at any given time is dictated by the total flow speed (sum of tidal and mean flow).

145   In this work the tilt noise band is used as a proxy to the bottom flow current speed that impacts the OBS structure. As a proxy to the tidal forcing of the deep ocean currents we will use the Sines harbor tide table from 10 to 28 of September 2007. This time period represents one cycle from spring to neap tide and back to the spring tide (Supplementary Table S1). The location of the Sines tide gauge is given in Figure 2.

3. Results and discussion

150   ### 3.1 Deep ocean current regime as inferred from OBS noise

We concentrate the OBS recorded noise analysis on two frequency bands, the short and the long-period (tilt noise) bands, for which we expected to see a strong tidal control if the noise is generated by deep ocean currents modulated by the tides. The interpretation of the results will follow the model of Voet et al., (2020).

Figure 5 illustrates the normalize spectrogram of NT OBS01 and NT OBS03, during the new moon spring tide (see

155   Figure 2 for location). At the new moon spring tide of 11 September 2007 (Tidal range of 2.8 meters measure in Sines tide gauge), NT OBS01 located at TAP, reveals a higher current flow speed during the flood tide, meaning that the superposition of flood tide and the permanent low-frequency flows exceeds the current flow speed threshold, the speed limit from laminar to turbulent flow, clearly recorded on the tilt noise domain between 20s and 60s, and on the broad band noise in the first noise domain (from 1-40Hz, shown by vertical lines on the spectrograms) and resulting the resonance scenario of harmonic

160   tremor in the time domain. During the ebb tide, which flow opposing, or at least not in phase, with the permanent low-

frequency flow, results in a reduced current flow speed and the resonance characteristics observed during the flood tide vanish.

NT OBS03 (Figure 5) shows a different noise pattern. During the ebb tide the resulting current flow speed exceeds the threshold speed scenario ensuing the harmonic tremor. However, during some periods of the flood tide, the harmonic

165 tremor is triggered due to episodic scenarios of higher current flow speed. The ebb tide and the low-frequency flows have similar directions. The flood tide has opposite direction with short episodes of some comparable direction.

During the first quarter moon neap tide (Figure 6), the tidal range measured in Sines was 0.7 meters, and NT OBS01 confirms that the permanent low-frequency flow dominates over the tide flow, however it is possible to see a contribution from the flood tide on harmonic tremors generation. The same characteristic observed during the spring tide is

170 observed during the neap tide, the low-frequency flow has comparable direction with flood tide and contrary to the ebb tide. In the same period NT OBS03 shows a pattern of low-frequency flow domination and the current flow speed threshold is never reached and the harmonic tremors are not trigger.

After the full moon (26 September 2007) the spring tide has tidal range of 3.5 meters, measured at Sines (28 September 2007, Figure 7). The tide flow in OBS01 continues to dominated during the flood tide and had a lesser influence

175 during the ebb tide. The same flow pattern was observed during both spring tides (11 and 28 September 2007). The permanent low-frequency flow shows similar directions with flood tide and opposed to the ebb tide (see supplementary file OBS01). On OBS03, at Marques de Pombal plateau, shows a similar flow pattern where the tide flow dominated during the ebb tide and in some smaller periods during flood tide. See supplementary file to infer all spectrograms from 10 to 28 September 2007.

180 We show that the ocean bottom flow as inferred from the tilt noise is not always a function of the tidal forcing. Instead it is shown that the ocean bottom has a flow regime that may have two contributions, the permanent low frequency current and the tidal current, as mentioned in Voet et al., (2020). The recorded tilt noise displays the balance between these two currents along the full tidal cycle, between neap tides and spring tides. From this flow pattern, it is possible to highlight that the most relevant parameter to the OBS noise recorded is the resulting current flow speed due to both currents or just

185 one of them. In Figure 1, during the neap tide of 19 October 2007, with a tidal range of 0.8 m (measured in Sines), it was possible to observe harmonic tremor features for as long as 24 hours in NT OBS01. The permanent low-frequency flow was the trigger of the resonance state, but a tidal modulation can be inferred.

Zooming-in on the harmonic tremor, as an example, on the 11 September it is possible to observe, during the flood tide, that every OBS component that has a resonant frequency inside the first noise domain starts to resonate (Figure 8). That

190 is the case of the head buoy rope, flagpole, radio antenna and the OBS package. The head buoy rope is tied directly to the titanium tubing mainframe of the OBS and held taut by the syntactic foam float. The flagpole and radio antenna have a rigid connection with the titanium frame. The seismic sensor, with a gimbled system, has a firm connection to the titanium mainframe and is pressed against the anchor (see Figure 3).

Natural Hazards
and Earth System
Sciences
Discussions

3.2 Harmonic tremor structure

From the spectrogram, which highlights the harmonic tremor, we conclude that when the current flow speed threshold is reach for each different OBS component, the first energetic resonance is due to the head buoy rope fundamental frequency (R1), afterwards the rope overtones (R2, R3 and R4) and radio antenna (A) and finally the flagpole (F) eigen-vibrations. Before and after the harmonic tremor (Figure 8, (1) and (6)), the dominant signal (C) is the natural frequency of OBS-sediments coupling, between 5.5 and 5.7Hz, observed during the entire recording period of the campaign. This signal is easily detected between the periods of 7h to 9h and from 16h to 19h on upper spectrogram.

The head buoy rope fundamental frequency (R1) starts to vibrate around 9h05m. The current flow causes the tensioned cable to strum (Stahler et al., 2018). At 9h15m, the head buoy rope overtones (R2, R3 and R4) start to emerge at integer multiples of the fundamental frequency. During this period the von Kármán vortex shedding off the rope is at a frequency lower than the resonance frequency of the rope and is observed the phenomena of frequency-gliding. At the same time the radio antenna (A) starts to resonate a minor frequency-gliding is observed. At 9h40m, four signals from the head buoy rope are visible, during frequency-gliding, with 0.92Hz, 1.84Hz, 2.76Hz and 3.68Hz, different from the values reported by Stahler et al., (2018) probably due to different rope length or speed current observed. The OBS-sediments coupling (C) is amplified at this time with a frequency around 5.7 Hz. The current flow speed at 10h00m initiated a new effect called wake or lock-in (Skop and Griffin, 1975; Griffin, 1985 and described at Stahler et al., 2018), denominated mode-locking frequency, stable until 14h00m, which is boosted when vortex shedding frequency is equal or close to the resonant frequency of the rope and radio antenna. At 10h30m, the flagpole eigen-vibrations begins, without any frequency gliding, and keeps the signal until 13h30m. Between (3) 10h50m and (4) 13h10m (Figure 8), for example, it is possible to identify the flagpole signal (F) with 1.45Hz, radio antenna (A) at 6.4Hz and the fundamental and overtones of the head buoy rope (R1 around 1.17Hz, R2 near 2.34Hz, R3 at 3.51Hz and R4 around 4.68Hz). At (5) 15h30m, R1, R2, R3 and R4 have a noticeable decrease of both amplitude and frequency due to the decrease of current flow speed. Around (6) 18h00m the OBS returns to its natural state and the main observed signal is the natural frequency of the OBS-sediments coupling.

During the NEAREST campaign in 2007, twenty-four OBS were deployed and analysed. Most of the OBS were deployed in areas where the current flow speed was not enough to trigger the harmonic tremors (Corela PhD, 2014). However, NT OBS04 (see Figure 2 for location) was deployed in an area where the current flow speed initiated a more energetic phenomena, where the transition to strong tremor increase the amplitude and the fundamental frequency of the head buoy rope and enlarged the number of overtones, and the mode-locking observed previously is no longer present (Figure 9). This phenomenon was observed, for example, during two period of 26 January 2008, the first between 11h and 13h, and the second between 22h40m and 24h due to strong non-linear interactions in the presence of strong currents.

In 2021, a new Broadband OBS type was deployed at the same location of NT OBS04 in order to study the DUNE OBS behaviour in a location where strong current flow speed is expected from previous analysis. The deployment period took place from May until October 2021. Searching for periods of strong tilt noise and associated noise in the first short-

period domain, as an example, during the 21 September 2021 (Figure 10), the harmonic tremors were not triggered because the radio antenna, flagpole and head buoy rope were isolated from vibrations and safely stowed inside the OBS shell (see

230   Figure 5), however strong tilt noise and the natural frequency OBS-sediments coupling were observed has expected. The 5 seconds noise is the second microseism noise associated with ocean swell.

In Figure 11 is show the behaviour of the new OBS during the campaign with low, moderate and strong current flow speed highlighted in the OBS-sediments coupling amplitude around 3.8Hz.

From the spectrogram, of the stronger current flow speed, it is possible to infer that the natural frequency of the

235   OBS-sediments coupling is amplified in amplitude with a lateral frequency distribution around 3.8Hz, similar to the observed in LOBSTER OBS in 2007. This new design, however, is still highly exposed to the current flow, however with lesser constrains when compared with the NT OBS04. Later iterations of this design are aimed on mitigating the natural frequency of the OBS-sediments coupling and the tilt noise on the OBS outer shell design.

240   **4. Conclusions**

Analysing seismic data recorded by OBS in the Gulf of Cadiz we showed that both the short-period (0.5Hz-40Hz) and long-period (20-60s) noise bands have an environmental origin of deep ocean currents. However, each site is unique in terms of depth, currents and topography. In this work we show that the ocean bottom flow as inferred from the tilt noise is not always dominated by the tidal forcing, but rather that the ocean bottom has a flow regime that may have two independent

245   contributions, the permanent low frequency current and the tidal current. The recorded noise displays the balance between these two currents along the full tidal cycle, between neap and spring tides and depends on the direction of each flow and the final combined current flow speed.

In the short-period noise domain we investigated in detail the harmonic tremor band (0.5Hz-6.5Hz) and showed that all the mechanical elements of the OBS that are not essential for recording at sea bottom do resonate when the current speed

250   reaches some threshold. Noise is shown on spectrograms by nearly constant frequency bands and by broadband spectral lines.

These findings support the interpretation that the strongest harmonic tremors are the result of the strumming of head-buoy rope on the LOBSTER design (Stahler et al., 2018; Essing et al., 2021) and confirmed that the radio antenna, flagpole and OBS-sediment coupling are also excited by the current flow speed when the laminar flow became turbulent in

255   each component. The head buoy rope's fundamental frequency and respective overtones exhibit frequency-gliding. The radio antenna also exhibits it, but with a lesser amplitude and the flagpole with no visible frequency-gliding. When the frequency of vortex shedding is near or identical to the resonance frequency of the different components we observe the mode-locking frequency. These characteristics are reported in different studies, however the strumming rope frequencies reported in this study are different from the reported previously (e.g. Stahler et al., 2018; Essing et al., 2021).

260   Our study provides additional support for another noise regime, without clear mode-locking frequency, when strong current flow actuates on the OBS. In NT OBS04 the observed harmonic tremor starts with frequency gliding but never reach

the mode-locking frequency state. The observed harmonic tremor increases the amplitude and enlarged the number of overtones.

The new DUNE OBS, deployed at the same position of the NT OBS04, with head buoy rope and floating device,
265 flagpole, radio antenna inside the OBS structure does not show any evidence of the harmonic tremors neither broadband noise observed on the LOBSTER OBS in the first noise domain. The observed signal is the resonance of the natural frequency of the OBS-sediments coupling which show an increase of the amplitude signal during the periods of high current flow speed with lateral frequency distribution. In the long-period noise domain, the tilt noise still needs to be mitigated. Research into solving this problem is already in progress at IDL and further work needs to be carried out to establish
270 improvements in OBS design. Future work should focus in changing the seismic sensor position and disconnected from the OBS structure in a smaller package. This action should solve the natural frequency of the OBS-sediments coupling problem and mitigate the tilt noise.

It should be noted that more modern deployment protocols for LOBSTER-type OBS already require that the head-buoy and rope are only free to leave the OBS frame after the anchor is release for ascent.

275 **References**

Alfred-Wegener-Institut, Helmholtz-Zentrum fur Polar- und Meeresforschung.: DEPAS (Deutscher Gerate-Pool fur amphibische Seismologie): German Instrument Pool for Amphibian Seismology, Journal of largescale research facilities, 3, A122, doi:10.17815/jlsrf-3-165, 2017.

Ardhuin, F., Gualtieri, L., and Stutzmann E.: How ocean waves rock the Earth: Two mechanisms explain microseisms with
280 periods 3 to 300s, Geophys. Res. Lett. 42, no. 3, 765–772, doi:10.1002/2014GL062782, 2015.

Bazin, S., Feuillet, N., Duclos, C., Crawford, W., Nercessian, A., Bengoubou-Valérius, M., Beauducel, F. and Singh, S. C.: The 2004–2005 Les Saintes (French West Indies) seismic aftershock sequence observed with ocean bottom seismometers, Tectonophysics 489, 91–103, doi: 10.1016/j.tecto.2010.04.005, 2010.

Bowden, D. C., Kohler, M.D., Tsai, V. S. and Weeraratne, D. S.: Offshore Southern California lithospheric velocity structure
285 from noise cross-correlation functions, J. Geophys. Res. Solid Earth, 121, doi:10.1002/2016JB012919, 2016.

Bromirski,, P. D., Duennebier, F. K., and Stephen, R. A.: Midocean microseisms. Geochem. Geophys. Geosys. 6, no. 4, doi:10.1029/2004GC000768, 2005.

Civiero, C., Strak, V., Custódio, S., Silveira, G., Rawlinson, N., Arroucau, P., Corela, C.: A common deep source for upper-mantle upwellings below the Ibero-western Maghreb region from teleseismic P-wave travel-time tomography, Journal of
290 Geophysical Research: Solid Earth, 124, 1781-1801, doi:10.1029/2018JB016531, 2018.

Civiero, C., Custódio, S., Rawlinson, N., Strak, V., Silveira, G., Arroucau, P., Corela, C.: Thermal nature of mantle upwellings below the Ibero-western Maghreb region inferred from teleseismic tomography, Earth and Planetary Science Letters, 499, 157-172, doi: 10.1016/j.epsl.2018.07.024, 2019.

Corela, C.: Ocean bottom seismic noise: applications for the crust knowledge, interaction ocean-atmosphere and
295 instrumental behavior. PhD thesis – Science Faculty of Lisbon University, http://hdl.handle.net/10451/15805, 2014.

Corela, C, Silveira, G., Matias, L., Schimmel, M. and Geissler, W.: Ambient seismic noise tomography of SW Iberia integrating seafloor and land-based data, Tectonophysics, 700-701, 131-149, doi: 10.1016/j.tecto.2017.02.012, 2017.

Díaz, J., Gallart, J., and Gaspà, O.: Atypical seismic signals at the Galicia Margin, North Atlantic Ocean, related to the resonance of subsurface fluid-filled cracks, Tectonophysics 433, 1–13, doi: 10.1016/j.tecto.2007.01.004, 2007.

300 Doran, A. K., and Laske, G.: Infragravity waves and horizontal seafloor compliance, J. Geophys. Res. 121, no. 1, 260–278, doi:10.1002/2015jB012511, 2015.

Duennebier, F. K., Blackinton, J. G., and Sutton, G.: Current-Generated Noise Recorded on Ocean Bottom Seismometers, Marine Geophys. Res. 5, 109-115, doi: 10.1007/BF00310316, 1981.

Duennebier, F. K., and Sutton, G. H.: Fidelity of ocean bottom seismometers, Mar. Geophys. Res., 17(6), 535–555, doi:
305 10.1007/BF01204343, 1985.

Essing, D., Schlindwein, V., Schmidt-Aursch, M. C., Hadziioannou, C. and Stähler, S. C.: Characteristics of Current-Induced Harmonic Tremor Signals in Ocean-Bottom Seismometer Records, Seismol. Res. Lett. 92(5), 3100-3112, doi: 10.1785/0220200397, 2021.

Franek, P., Mienert, J., Buenz, B., and Géli, L.: Character of seismic motion at a location of a gas hydrate bearing mud
310 volcano on the SW Barents Sea margin, J. Geophys. Res. 119, 6159–6177, doi: 10.1002/2014JB010990, 2014.

Garrett, C., and Kunze, E.: Internal Tide Generation in the Deep Ocean, Ann. Rev. Fluid Mech., 39, 57–87, doi: 10.1146/annurev.fluid.39.050905.110227, 2007.

Geissler, W.H., Matias, L., Stich, D., Carrilho, F., Jokat, W., Monna, S., IbenBrahim, A., Mancilla, F., Gutscher, M.-A., Sallarès, V., Zitellini, N.: Focal mechanisms for sub–crustal earthquakes in the Gulf of Cadiz from a dense OBS deployment,
315 Geophys. Res. Lett. 37, L18309. Doi: 10.1029/2010GL044289, 2010.

Griffin, O. M.: Vortex-induced vibrations of marine cables and structures, Technical Report, Naval Research Lab, Washington, D. C., available at http://www.dtic.mil/docs/citations/ADA157481, 1985.

Kovachev, S. A., Demidova, T. A., and Son'kin, A. V.: Properties of noise registered by Pop-Up Ocean Bottom Seismographs, Journal of Atmospheric and Oceanic Technology, 883-888, doi: 10.1175/1520-
320 0426(1997)014<0883:PONRBP>2.0.CO;2, 1997.

Lewis, B. and Tuthill, J.: Instrumental Waveform Distortion on Ocean Bottom Seismometers, Marine Geophys. Res. 5, 79-86, doi: 10.1007/BF00310313, 1981.

Longuet-Higgins, M. S.: A theory of the origin of microseisms, Phil. Trans. Roy. Soc. Lond. A 243, no. 857, 1–35, doi:10.1098/rsta.1959.0012, 1950.

325 Loureiro, A., Afilhado, A., Matias, L., Moulin, M., Aslanian, D.: Monte Carlos approach to assess the uncertainty of wide-angle layered models: Application to the Santos Basin, Brazil, Tectonophysics 683, 286-307, doi: 10.1016/j.tecto.2016.05.040, 2016.

Meier, M., and Schlindwein, V.: First in situ seismic record of spreading events at the ultraslow spreading Southwest Indian ridge, Geophys. Res. Lett. 45, 10,360–10,368, doi: 10.1029/2018gl079928, 2018.

330 Monigle, P. W., Bohnenstiehl, D. R., Tolstoy, M., and Waldhauser, F.: Seismic tremor at the 9_500N East Pacific Rise eruption site, Geochem. Geophys. Geosys. 10, doi: 10.1029/2009GC002561, 2009.

Nikurashin, M., and Ferrari, R.: Radiation and dissipation of internal waves generated by geostrophic flows impinging on small-scale topography: Theory, J. Phys. Oceanogr., 40, 1055–1074, doi: 10.1175/2009JPO4199.1, 2010a.

Nikurashin, M., and Ferrari, R.: Radiation and dissipation of internal waves generated by geostrophic flows impinging on
335 small-scale topography: Application to the Southern Ocean, J. Phys. Oceanogr., 40, 2025–2042, doi: 10.1175/2010JPO4315.1., 2010b.

Pontoise, B., and Hello, Y.: Monochromatic infra-sound waves recorded offshore Ecuador: Possible evidence of methane release, Terra Nova 14, 425–435, doi: 10.1046/j.1365-3121.2002. 00437.x, 2002.

Ramakrushana Reddy, Dewangan, T. P., Arya, L., Singha, P. and Kamesh Raju, R. A.: Tidal triggering of the harmonic
340 noise in ocean-bottom seismometers, Seismol. Res. Lett. 91, 803–813, doi: 10.1785/0220190080, 2020.

Silva, S., Terrinha, P., Matias, L., Duarte, J. C., Roque, C., Ranero, C. R., Geissler, W. and Zitellini, N.: Micro-seismicity in the Gulf of Cadiz: Is there a link between micro-seismicity, high magnitude earthquakes and active faults?, Tectonophysics, 717, 226-241, doi: 10.1016/j.tecto.2017.07.026, 2017.

Stähler, S. C., Schmidt-Aursch, M. C., Hein, G., and Mars, R.: A self-noise model for the German DEPAS OBS pool.
345 Seismol. Res. Lett. 89, 1838–1845, doi: 10.1785/0220180056, 2018.

Skop, R. A., and Griffin, O. M.: On a theory for the vortex-excited oscillations of flexible cylindrical structures, J. Sound Vib. 41, no. 3, 263–274, doi: 10.1016/S0022-460X(75)80173-8, 1975.

Sumer, B. M., and Fredsøe, J.: Hydrodynamics around Cylindrical Structures, P. Liu (Editor), Vol. 12, Advanced Series on Ocean Engineering, World Scientific, Singapore, 1999.

350 Sutton, G. H., Duennebier, F. K., and Iwatake, B.: Coupling of Ocean Bottom Seismometers to Soft Bottom, Marine Geophys. Res, 5, 35 51, doi: 10.1007/BF00310310, 1981a.

Sutton, G. H., Duennebier, F. K., Iwatake, B., Tuthill, J., Lewis, B., and Ewing, J.: An Overview and General Results of the Lopez Island OBS Experiment, Marine Geophys. Res. 5, 3 34, doi: 10.1007/bf00310309, 1981b.

Sutton, G. H., and Duennebier, F. K.: Optimum design of ocean bottom seismometers, Mar. Geophys. Res. 9, no. 1, 47–65,
355 doi: 10.1007/BF00338250, 1987.

Trehu, A. M. and Solomon, S. C.: Coupling parameters of the MIT OBS at two nearshore sites, Marine Geophys. Res. 5, 69-78, doi: 10.1007/BF00310312, 1981.

Trehu, A. M.: Coupling of Ocean Bottom Seismometers to Sediment: Results of Tests with the U.S. Geological Survey Ocean Bottom Seismometer, Bull. Seism. Soc. Am. 75, 271-289, 1985a.

360 Trehu, A. M.: A Note on the Effect of Bottom Currents on an Ocean Bottom Seismometer, Bull. Seism. Soc. Am. 75, 1195-1204, 1985b.

Natural Hazards
and Earth System
Sciences
Discussions

Tolstoy, M., Vernon, F. L., Orcutt, J. A. and Wyatt, F. K.: Breathing of the seafloor: Tidal correlations of seismicity at Axial volcano, Geology 30, 503–506, doi: 10.1130/0091-7613(2002)030<0503:BOTSTC>2.0.CO;2, 2002.

Ugalde, A., Gaite, B., Ruiz, M., Villaseñor, A. and Ranero, C. R.: Seismicity and noise recorded by passive seismic monitoring of drilling operations offshore the Eastern Canary Islands, Seismol. Res. Lett. 90, 1565–1576, doi: 10.1785/0220180353, 2019.

Voet, G. Alford, M. H., and MacKinnon, J.: Topographic form drag on tides and low-frequency flow: Observations of nonlinear Lee Waves over a tall submarine ridge near Palau, Journal of Physical Oceanography, 50, 1489-1507, doi: 10.1175/ JPO-D-19-0257.1, 2020.

Webb, S.C.: Broadband seismology and noise under the ocean, Rew.Geophys., 36 1, 105–142, doi: 10.1029/97RG02287, 1998.

Webb, S. C.: The Earth's "hum" is driven by ocean waves over the continental shelves, Nature 445, no. 7129, 754–756, doi:10.1038/nature05536, 2007.

Wessel, P., Smith, W. H. F., Scharroo, R., Luis, J. F., and Wobbe, F.: Generic Mapping Tools: Improved version released, Eos Trans. AGU 94, 409–410, doi: 10.1002/2013EO450001, 2013.

Zelikovitz, S. J. and Prothero, W. A.: The vertical response of an ocean bottom seismometer: analysis of the Lopez Island vertical transient tests, Marine Geophys. Res. 5, 53-67, doi: 10.1007/BF00310311, 1981.

Competing interests

The authors declare that they have no conflict of interest.

Data Resources

Supplemental material for this article includes a tide table from Sines and normalized spectrograms from 11 September 2007 (spring tide - new moon) to 28 September 2007 (spring tide -full moon). Figures for this article and supplemental material were created using Generic Mapping Tools (GMT) (Wessel et al., 2013) and ObsPy (Krischer et al., 2015). The LOBSTER OBS data, acquired in SW Iberia, near Portugal, is a contribution from project NEAREST FP6-2005-GLOBAL-4 (OJ 2005 C177/15). The new broadband OBS data were provided by DUNE project (PTDC/EAM-OCE/28389/2017) (Ocean Bottom Seismometer Main Page – DUNE Project (FCT) – Instituto Dom Luiz (ulisboa.pt)).

Acknowledgments

390   Geoforschungszentrum Potsdam (doi:10.17815/jlsrf-3-165). The authors are also grateful to the crew of RV *Mário Ruivo* for the excellent support during deployment and retrieval of OBS on cruise EMSO-PT 2021. This work was funded by Portuguese Fundação para a Ciência e a Tecnologia (FCT) I.P./MCTES through national funds (PIDDAC) – UIDB/50019/2020 -Instituto Dom Luiz (IDL).

395 **Figures**
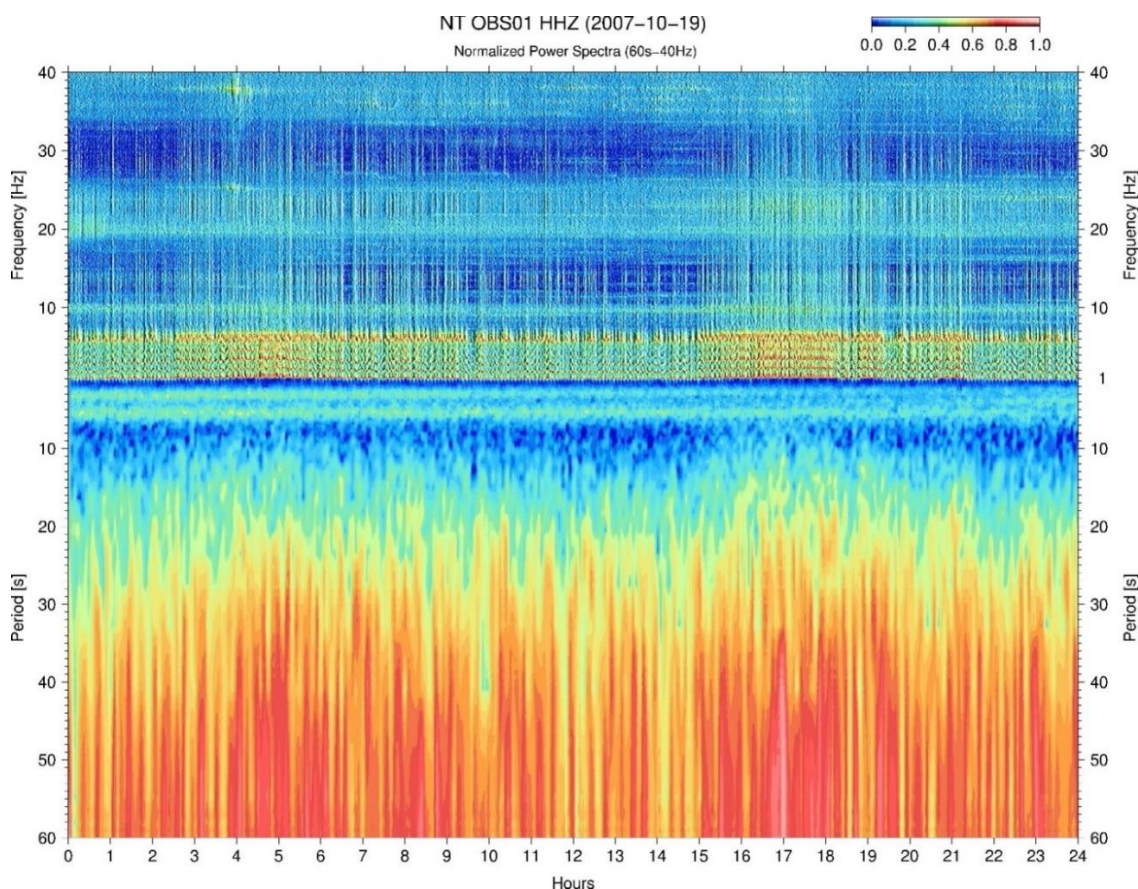
Figure 1 | Noise domain – Short-period band from 0.5Hz to 40Hz shows long-lasting harmonic tremor signals frequently observed in
400 spectrograms of OBS data with overlapping frequency content with earthquake detection between 1 and 6.5 Hz. The long-period band from 20s-60s shows the tilt noise and the microseisms noise band between 2s and 20s. The harmonic tremor, microseism and tilt noise are show in this particular OBS data records and are continuously observed in one-day spectrogram (OBS01). The spectrogram is made between 40Hz and 0.0167Hz, however, between 1Hz and 0.0167Hz converted to Period in seconds with linear axes.

405
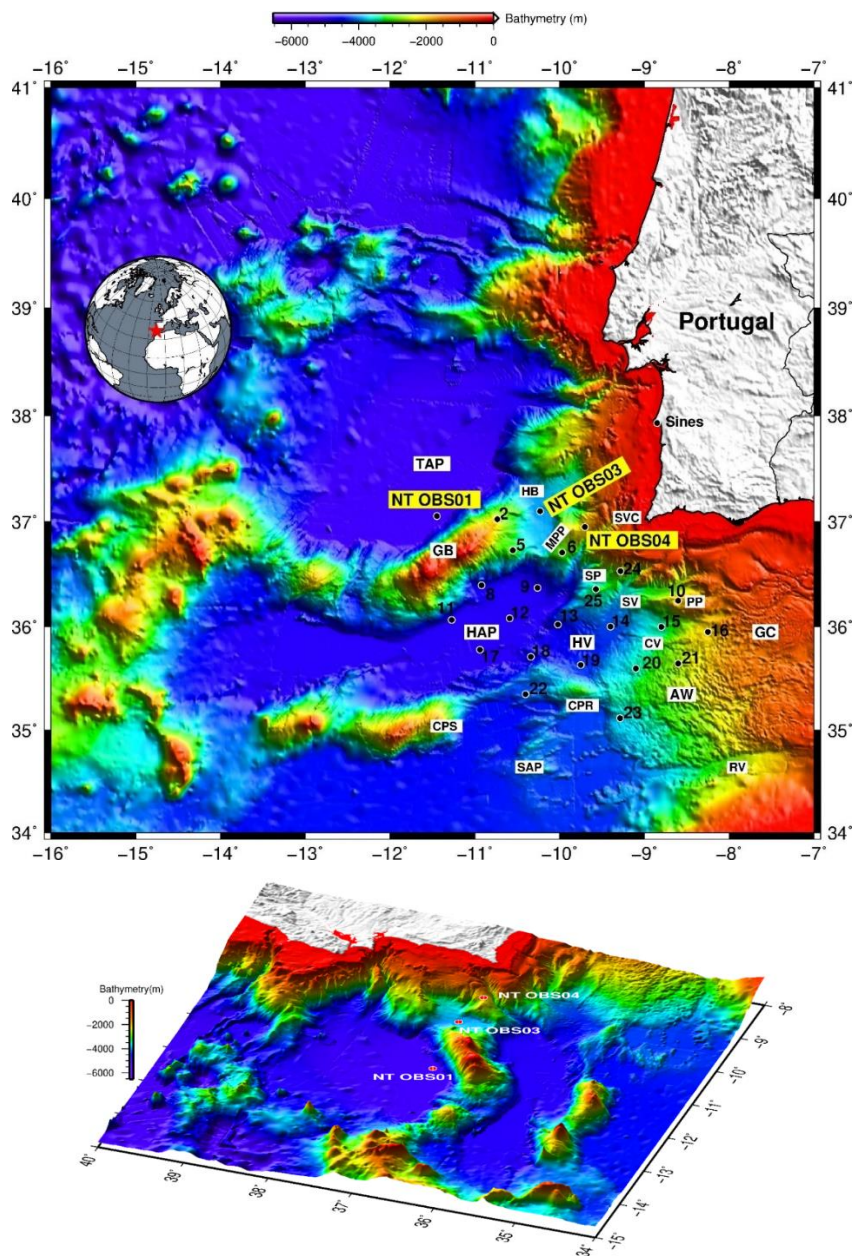
Figure 2 | LOBSTER OBS location - Deployment of 24 OBS (**1** represents OBS01, and so on) used in the NEAREST project. Main geographical features shown: TAP – Tagus Abyssal Plain; HB – D. Henrique Basin; GB - Gorringe Bank; MPP – Marquês de Pombal
410   Plateau; SVC – São Vicente Canyon; SP – Sagres Plateau; HAP – Horseshoe Abyssal Plain; SV – Sagres Valley; PP – Portimão Plateau; HV – Horseshoe Valley; CV – Cádiz Valley; GC – Gulf of Cádiz; SG – Strait of Gibraltar; CPR – Coral Patch Ridge; AW – Accretionary Wedge; CPS – Coral Patch Seamounts; SAP – Seine Abyssal Plain; RV – Rharb Valley. The OBS NT OBS01, NT OBS03 and NT OBS04 are used in this study (Wessel et al., 2013).
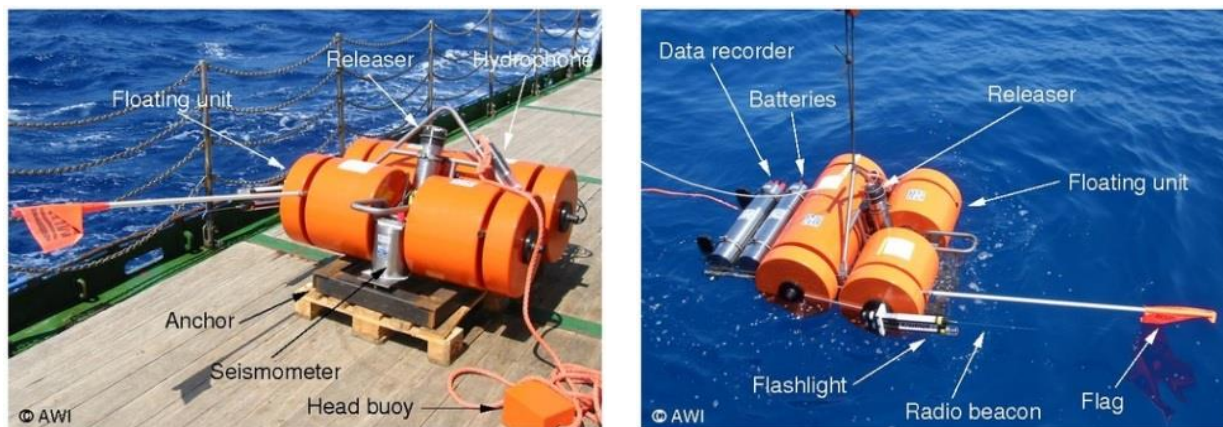
Figure 3 | NEAREST Lobster OBS used in NEAREST project. On the left: OBS on deck ready for deployment.
On the right: OBS suspended by the ship's crane, waiting for the deploy signal.
(*in* https://www.awi.de/en/science/geosciences/geophysics/methods-and-tools/refraction-seismology.html)


Figure 4 | DUNE OBS. New broadband OBS developed and build in Portugal with the new seismic sensor from GURALP Aquarius
(120s-100Hz) and a broadband hydrophone HTI-04-PCA. On the left DUNE OBS on free-fall in the water column.
On the right: Recovery of the DUNE OBS with the flag, radio and flashlight outside the orange shell. The deployment and recovery on
board Portuguese vessel, RV *Mário Ruivo* (IPMA).

15

435
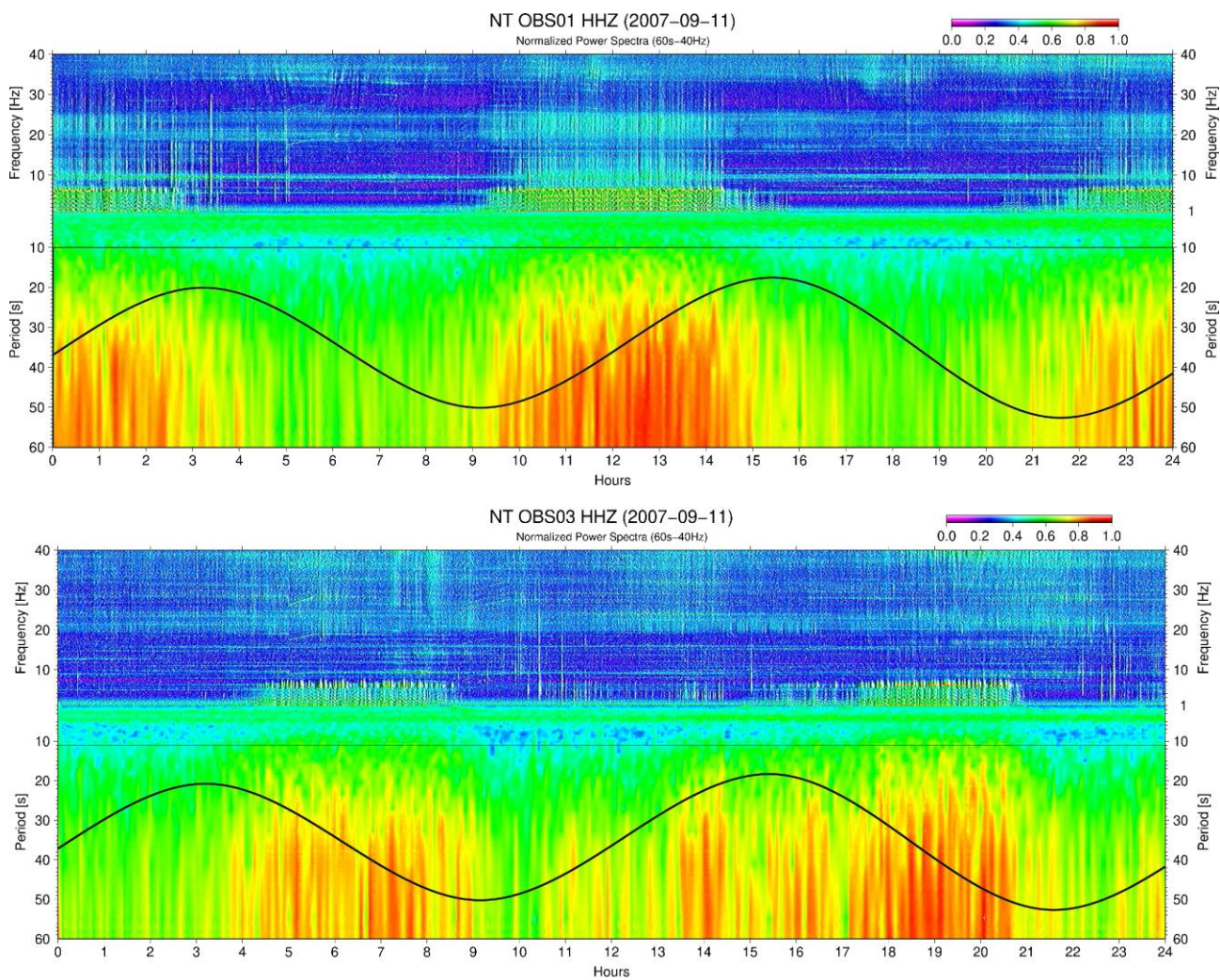
Figure 5 | Spring Tide at new moon – Spectrograms of OBS01 and OBS03 (11 September 2007) during the spring tide. The OBS shows different responds to the tide and low frequency current flows. During the spring tide the tidal range in Sines was 2.8 meters. The black line represents the periodic tide measured on that day. The minimum represents the low tide, the maximum high tide, the rising curve is the

440   flood tide and the falling the ebb tide.

445

450

455
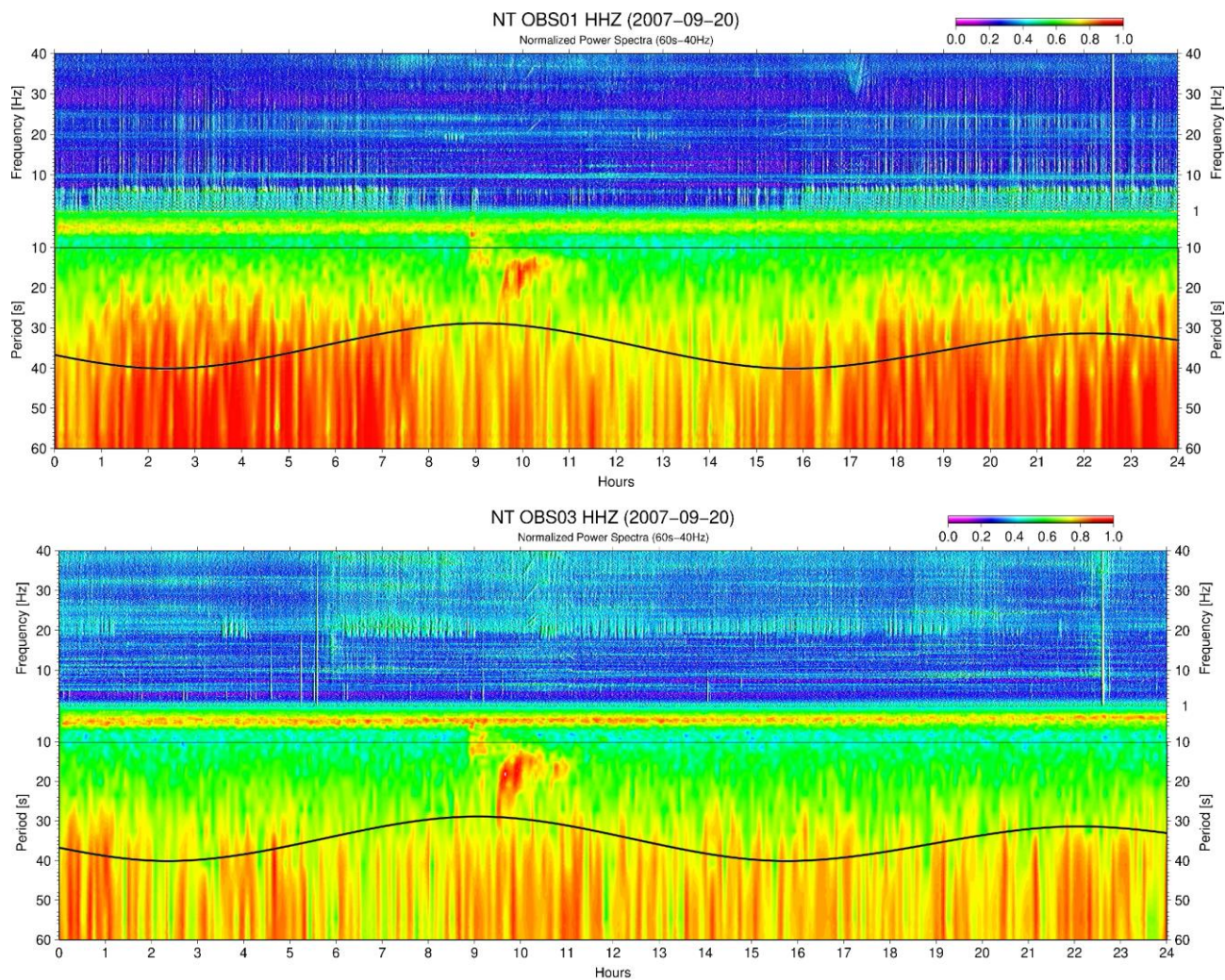
Figure 6 | Neap tide in quarter moon – OBS01 and OBS03 spectrograms during the neap tide period (20 September 2007). The permanent low-frequency flow dominates over the tide flow. The tidal range in neap tide was 0.7 meters (measured in Sines). In OBS03 is observe the whale singing between 20 and 24Hz.

460
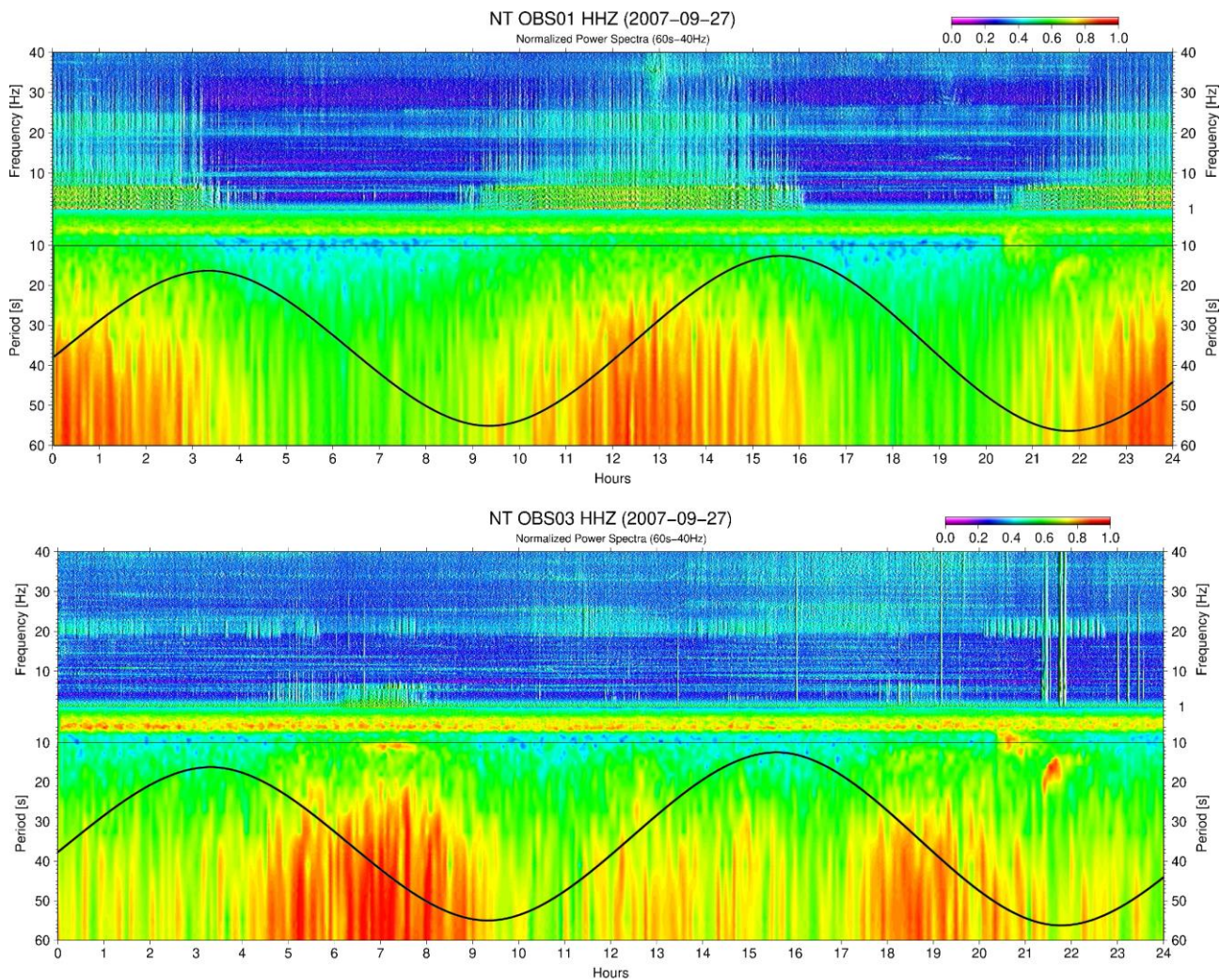
Figure 7 | Spring Tide at full moon – NT OBS01 and NT OBS03 spectrograms during the spring tide (28 September 2007). The OBSs show different respond to the energy balance between tide and permanent low frequency flows. The NT OBS01 during flood tide and NT OBS03 in ebb tide. During the spring tide, the tidal range was 3.5 meters (measured in Sines).

Natural Hazards
and Earth System
Sciences
Discussions

465
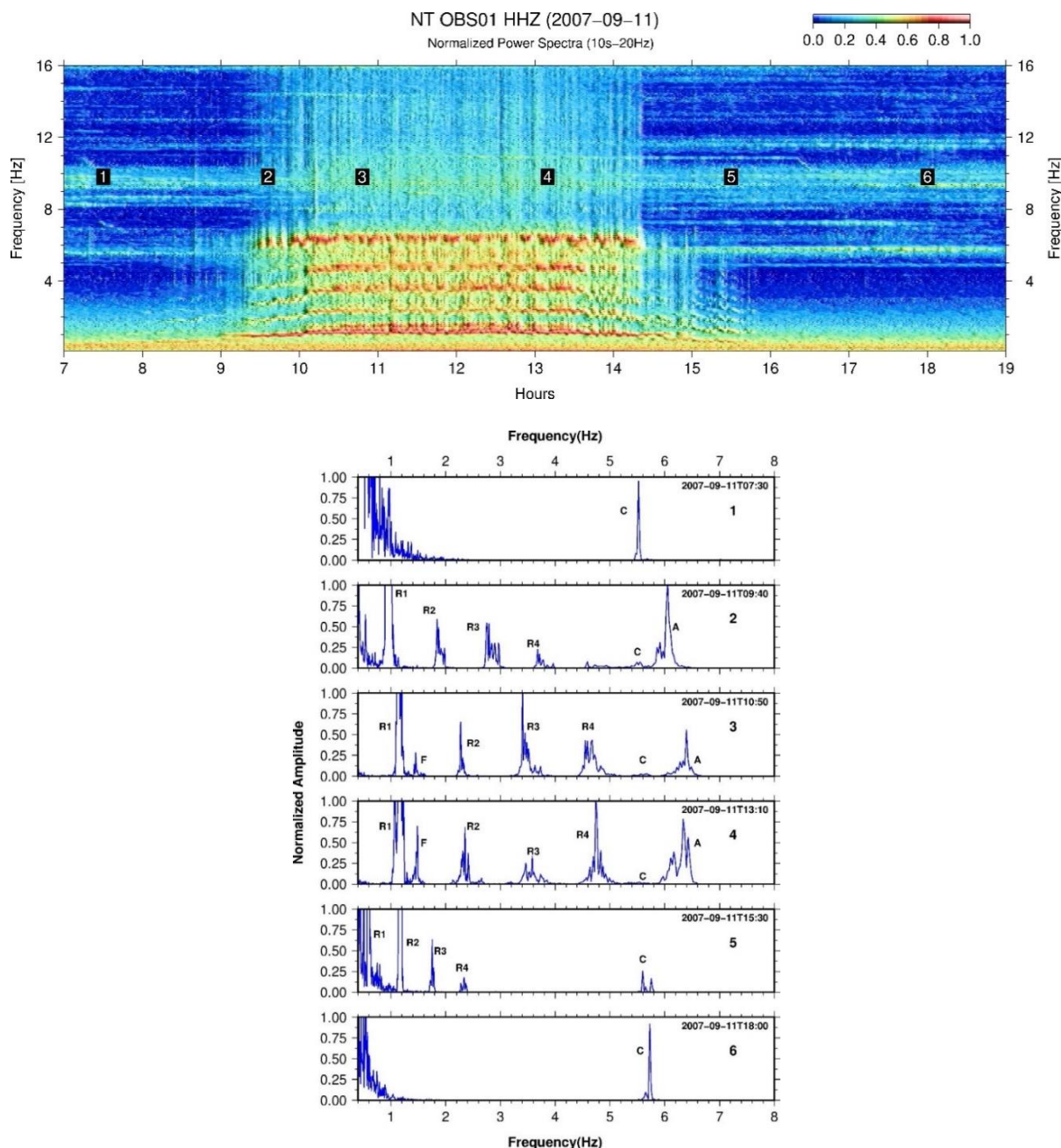
Figure 8 | Harmonic tremors– The prevailing signals before, during and after the harmonic tremor. The current flow speed describes in terms of (A) radio antenna, (F) flagpole, (R1) head buoy rope fundamental frequency, (R2) 2nd, (R3) 3rd, (R4) 4th overtones and (C) the

470　natural frequency of OBS-sediments coupling. At (1) 07h30m, before the harmonic tremors, with his normal vibration; (2) 09h40m during the period when the current flow speed threshold was reach and was observed frequency gliding in the head buoy rope; (3) 10h50m we observe mode-locking frequency on harmonic tremor; (4) 13h10m continues the previous situation in terms of frequency (mode-locking); (5) 15h30 the current flow speed is decreasing and was observed a frequency-gliding of the head buoy rope; (6) 18h30m the harmonic tremor is no longer active and the natural frequency of OBS-sediments coupling return to normal.
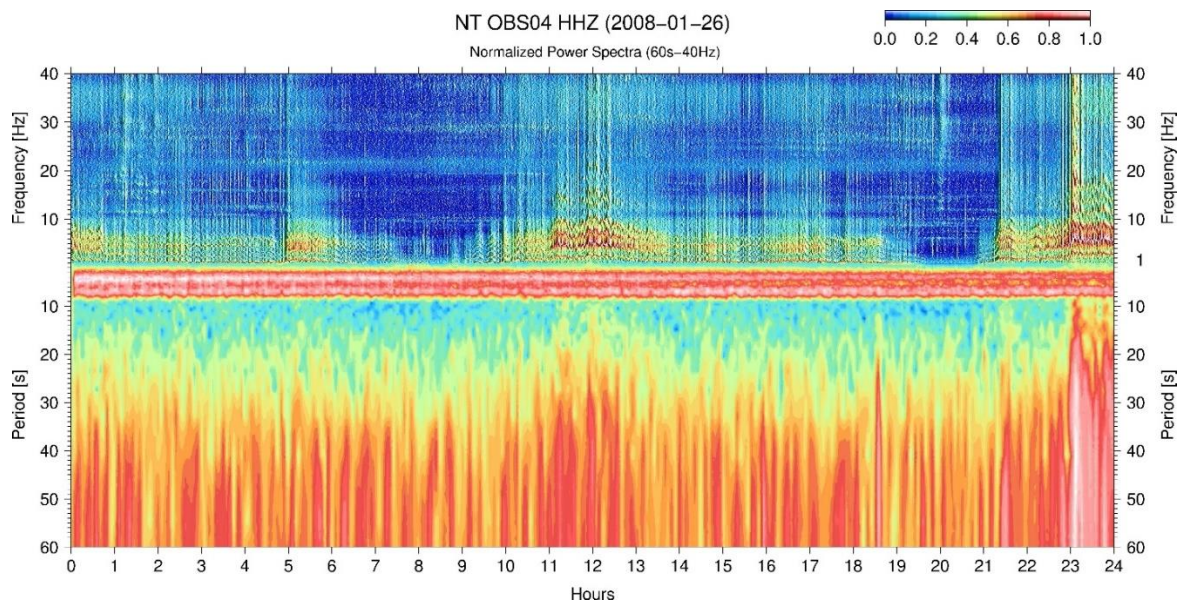
Figure 9 | Strong tremor. Between 11h and 13h and 23h and 24h it's possible to see the effect of the current flow speed on the head buoy rope.
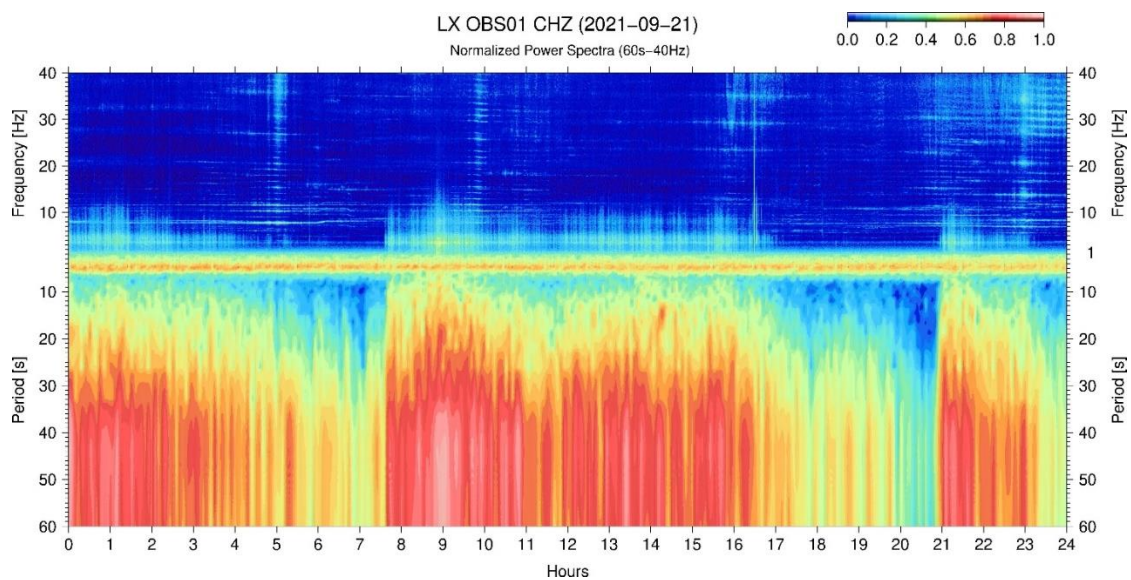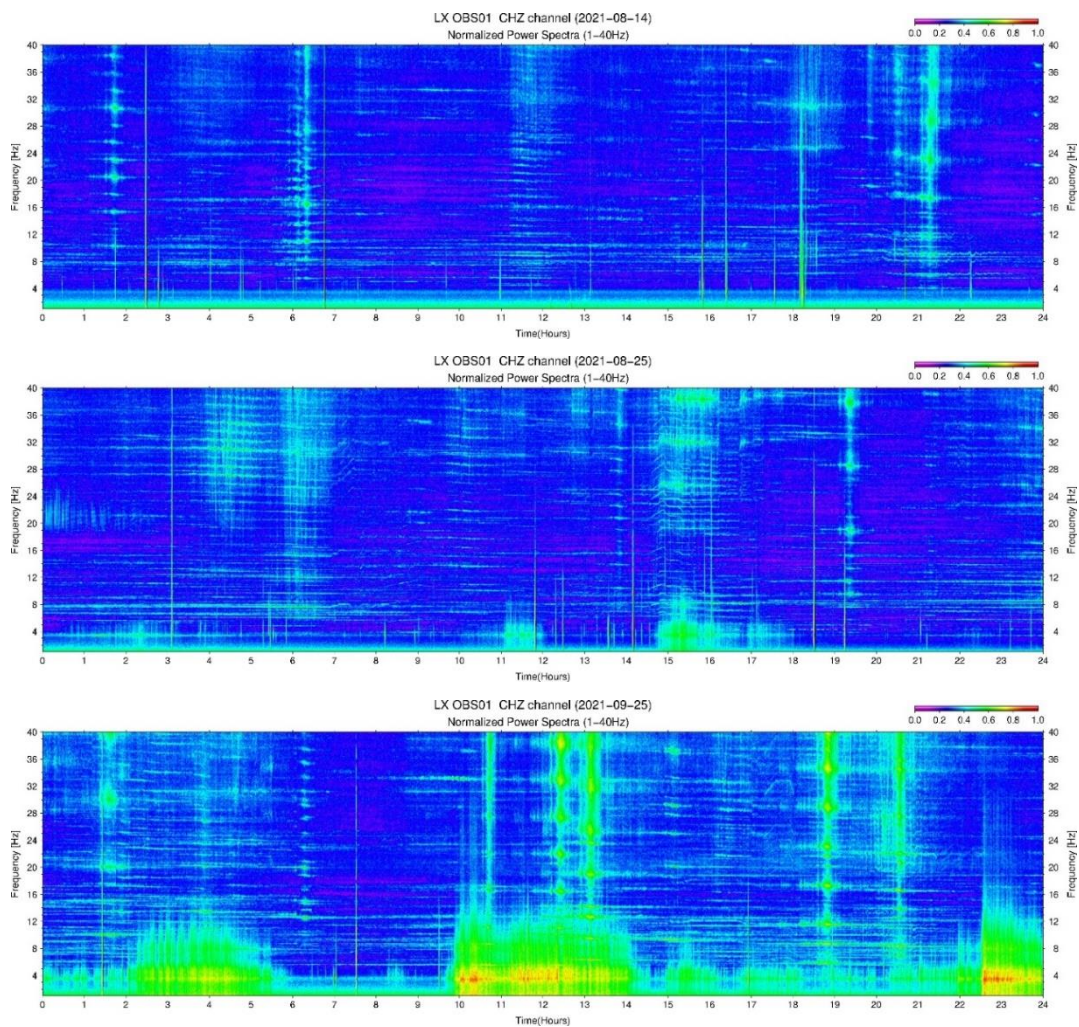

Figure 10 | New broadband OBS spectrogram. In this particular day a strong current flow scenario was observed during the 2021 campaign without harmonic tremors but with tilt noise.

Natural Hazards
and Earth System
Sciences
Open Access
Discussions
EGU

495

Figure 11 | Spectrograms from 1 to 40Hz. A low, moderate and high current flow speed during the 2021 campaign of the broadband OBS build at the University of Lisbon (Instituto Dom Luiz-IDL).